Published in final edited form as:
Anat Rec (Hoboken). 2013 January ; 296(1): 133–145. doi:10.1002/ar.22620.

Tensor Tympani Motoneurons Receive Mostly Excitatory Synaptic Inputs

THANE E. BENSON[1,*], **DANIEL J. LEE**[1,2], and **M. CHRISTIAN BROWN**[1,2]

[1]Eaton-Peabody Laboratory, Massachusetts Eye and Ear Infirmary, Infirmary, 243 Charles St., Boston, Massachusetts

[2]Department of Otology and Laryngology, Harvard Medical School, Boston, Massachusetts

Abstract

The tensor tympani is a middle ear muscle that contracts in two different situations: in response to sound or during voluntary movements. To gain insight into the inputs and neural regulation of the tensor tympani, we examined the ultrastructure of synaptic terminals on labeled tensor tympani motoneurons (TTMNs) using transmission electron microscopy. Our sample of six TTMNs received 79 synaptic terminals that formed 126 synpases. Two types of synapses are associated with round vesicles and form asymmetric junctions (excitatory morphology). One of these types has vesicles that are large and round (Lg Rnd) and the other has vesicles that are smaller and round (Sm Rnd) and also contains at least one dense core vesicle. A third synapse type has inhibitory morphology because it forms symmetric synapses with pleomorphic vesicles (Pleo). These synaptic terminals can be associated with TTMN spines. Two other types of synapse are found on TTMNs but they are uncommon. Synaptic terminals of all types form multiple synapses but those from a single terminal are always the same type. Terminals with Lg Rnd vesicles formed the most synpases per terminal (avg. 2.73). Together, the synaptic terminals with Lg Rnd and Sm Rnd vesicles account for 62% of the terminals on TTMNs, and they likely represent the pathways driving the contractions in response to sound or during voluntary movements. Having a high proportion of excitatory inputs, the TTMN innervation is like that of stapedius motoneurons but proportionately different from other types of motoneurons.

Keywords

middle ear muscle; acoustic reflex; vesicle morphometry; dense core vesicle; electron microscopy

INTRODUCTION

The tensor tympani and stapedius muscles are the two muscles that regulate sound transmission through the middle ear. In non-human mammals, both the tensor tympani and the stapedius contract in response to sound (Gelfand, 1984; Stach et al., 1984; Møller, 1984; Horner, 1986; van den Berge et al., 1990; Relkin et al., 2005). This contraction protects the inner ear from damage due to intense sounds and reduces the effects of noise masking. The muscles also contract during vocalization, swallowing and chewing (Salomon and Starr, 1963; Borg et al., 1984; Stach et al., 1984; Howell et al., 1986), perhaps to avoid self-stimulation that could lead to loss of sensitivity. The sound-evoked contraction and the other

[*]Correspondence to: Thane E. Benson, Eaton-Peabody Laboratory, Massachusetts Eye and Ear Infirmary, 243 Charles St., Boston, MA. Fax: 617-720-4408. Thane_Benson@meei.harvard.edu.

contractions make it likely that there are at least two pathways that excite the middle ear muscle systems.

The pathways causing activation of the middle ear muscles converge on the motoneurons as synaptic terminals. Stapedius motoneurons receive five types of synaptic terminals (Lee et al., 2008), the overwhelming majority of which contain vesicles that are round and are likely to provide excitatory input mediated by the neurotransmitter glutamate (Uchizono, 1965;Örnung et al., 1998; Torrealba and Carrasco, 2004; Rubio, 2004). Most of the remaining synaptic terminals, less than 20%, contain vesicles that are pleomorphic and are likely to provide inhibitory input. This synaptic profile is proportionately different from spinal α-motoneurons, which receive input predominantly from flattened/pleomorphic vesicle terminals (Conradi et al., 1979; Ichiyama et al., 2006). The synaptic profile onto tensor tympani motoneurons (TTMNs) has not previously been investigated. To examine the inputs and to gain insight into the neural control of the tensor tympani muscle, we investigated the ultrastructure of TTMN synaptic terminals.

Our study provides morphometric information on the synaptic vesicles of the inputs to TTMNs. For over a half-century, investigators of the auditory system have classified synaptic terminals according to whether the vesicles are round versus oval/flat, using visual inspection of terminals in the cochlear nucleus (Schwartz and Gulley, 1978; Cant and Morest, 1979; Treeck and Pirsig, 1979; Cant 1993; Benson et al., 1996; Rubio, 2004) and the superior olivary complex (Lenn and Reese, 1966; Schwartz, 1980). Similar approaches have been performed on motoneurons (Conradi et al., 1979; Ichiyama et al., 2006; Lee et al., 2008). In the cochlear nucleus, a further distinction can be made for round vesicles; those that are large, which disappear after removal of the auditory-nerve input (Treeck and Pirsig, 1979), and those that are small, which remain. Other than measurement of vesicles in a few terminals, little quantitative work has been done to establish what type of metrics can be used to separate terminals on motoneurons. We investigate, for terminals on TTMNs, whether quantitative rules can be established for separating synapses according to vesicle size and shape. The results demonstrate that the several common types can be separated by vesicle morphometry. Together with the two uncommon types of terminals, the results show that there is a large diversity of synaptic input to TTMNs, the majority of which has excitatory morphology.

MATERIALS AND METHODS

All experimental procedures on Sprague-Dawley rats were performed in accordance with the National Institutes of Health guidelines for the care and use of laboratory animals as well as approved animal care and use protocols at the Massachusetts Eye & Ear Infirmary. A total of four rats were used. In two rats used for combined light and electron microscopy, the methods were similar to our work on stapedius motoneurons (Lee et al., 2008), except that injections of 30% horseradish peroxidase were made into the tensor tympani muscle. After a survival time of 24 hr, the rats were reanesthetized and perfused with 0.1% sodium nitrite in physiologic saline followed by 0.5% paraformaldehyde and 1% glutaraldehyde in 0.1 M cacodylate buffer, which was then followed by 0.5% paraformaldehyde and 3% glutaraldehyde in buffer. The total fixation time was 2 hr. The brainstem was blocked, embedded in a gelatin-albumin mixture hardened with 2.3% glutaraldehyde, and sectioned (80 μm thickness, transverse plane) using a Vibratome. The sections were soaked in a solution of tetramethylbenzidine and ammonium heptamolybdate (Olucha et al., 1985) in 0.1 M phosphate buffer made hypertonic with dextrose. Hydrogen peroxide (0.3%, 1 mL/100 mL) was then added every five minutes for twenty minutes. The sections were moved to fresh incubation solution and H_2O_2 again added to allow a more dense reaction product with minimal crystal artifact. Selected sections with labeled TTMNs were treated overnight with

hypertonic OsO_4 (pH 5 at 3° C, Henry et al., 1985). The sections were stained en bloc with filtered 1% uranyl acetate (overnight at 3° C), dehydrated with methanol through propylene oxide, infiltrated with epoxy and flat-embedded between two transparent sheets of Aclar (Pro Plastics, Wall, NJ). In two other rats used for light microscopy alone, Fluorogold was used as the tracer and animals were perfused with 4% paraformaldehyde. These sections were processed with an anti-Fluorogold antibody (Fluorochrome, Denver, CO; see Mukerji et al., 2009).

For labeled neuron measurements, the somata were outlined using a camera lucida attachment on a light microscope. The soma area, maximum diameter, and minimum diameter were measured using ImageJ. The six labeled TTMNs selected for examination under the electron microscope consisted of four neurons (N1, N2, N5, and N6) from the first rat and two (N3 and N4) from the second rat. After documentation with the light microscope, ultrathin serial sections of the same material were taken. The section thickness was presumed to be 80 nm because of the silver-gold color of the sections (Sakai, 1980). The sections were examined with the transmission electron microscope and a correlation between the light- and electron-microscopic images was made.

To qualify as a synapse, three criteria were required: a cleft between pre- and postsynaptic membrane, postsynaptic dense material, and presynaptic vesicles. The criterion of postsynaptic dense material could be replaced by a cistern. We determined whether dense core vesicles were present in any part of the terminal for serially sectioned material. For terminals in which dense core vesicles were deemed not present, 4-18 sections were examined. For synapses for which all sections were available, we determined the total number of vesicles per synapse (counted within 0.5 μm of the presynaptic membrane adjacent to the density in all sections containing the density). The percent coverage of the cell bodies was made using one nucleus-containing section for each of the five somata. The distinction between soma and proximal dendrite was made on the basis of tapering of the soma into the dendrite and whether organelles are oriented circumferentially around the nucleus in the soma vs. parallel to the axes of dendrites.

Morphometric data on synaptic vesicles were obtained from images of 21,000-25,000× original magnification. Vesicles were traced along the outer edges of their membranes using a digitizing tablet. ImageJ was used to compute vesicle area and circularity ($4\pi[\text{area}/\text{perimeter}^2]$) (Montero and Bribiesca, 2009). This definition of circularity is similar to that used previously to distinguish round vs. nonround synaptic vesicles (Berrebi and Spirou, 1998) except that the measure we have used ranges from 0 to 1 (for a circle, circularity is 1.0 and for an ellipse with a major axis twice that of its minor axis, it is 0.84). Vesicles were measured in up to six sections per synapse, and data for all available synapses were combined for each terminal for Fig. 4. Due to the fact that vesicular data fell over a wide range, it was necessary to analyze a large number of vesicles for each terminal (18-103 vesicles, all of which were within 250-800 nm from the presynaptic membrane adjacent to the density). We excluded from the data set 10 terminals with fewer than 18 vesicles; these terminals were usually small, partially documented terminals at the beginning or end of the series of sections, or in one instance a terminal whose volume was taken up by a mitochondrion leaving little space for vesicles. As described by Doucet et al. (2009), the k-means clustering algorithm (implemented as the *kmeans* function in MATLAB) was used to provide an objective method for dividing the morphometric data. Data were normalized on a scale from 0 to 1 before the analysis was performed.

In order to determine whether terminals formed several synapses, each terminal was assigned an identifier and followed through the serial sections. A terminal was considered

partially sectioned if it continued beyond the sections available and completely sectioned if its apposition with the TTMN tapered off to a small process within the available sections.

En face representations of terminal appositions with the TTMNs were made by tracing the apposition in each section and staggering the drawing by the section thickness (80 nm). Appositions were measured in sections containing the synaptic density. If a terminal gave rise to multiple synapses, the one with the longest apposition was chosen for measurement. Minute glial processes (less than 0.05 μm) that intervened for a portion of the apposition of the largest terminals were ignored for the measurement.

The areas of individual synapses were determined using serial sections. If a terminal had multiple synapses, the largest one was chosen for measurement. In each section, the length of the synaptic cleft was measured using Image J. To calculate area, the lengths (μm) were summed and multiplied by the section thickness (80 nm). Statistical tests, means, and standard errors (SE) were computed using Kaleidagraph® software.

RESULTS

Labeled TTMNs and Their Features

After injections of tracer into the tensor tympani muscle, labeled TTMNs are found in the brainstem on the side ipsilateral to the injected muscle. They are located in a region ventrolateral to the trigeminal motor nucleus (Fig. 1A) in agreement with earlier studies in rat (Spangler et al., 1982; Rouiller et al., 1986; Billig et al., 2007; Reuss et al., 2009) and in other species (Shaw and Baker, 1983; Strutz et al., 1988; Mukerji et al., 2009). Using four rats, we measured 92 labeled neurons. For our labeled neurons, the average major axis diameter was 31.1 μm (SE 0.86) and the average minor axis diameter was 14.7 μm (SE 0.54); these dimensions are similar to earlier studies (Spangler et al., 1982; Rouiller et al., 1986; Billig et al., 2007). The six TTMNs selected for examination in the electron microscope (Table 1, Fig. 1A) had somata sizes that span the range observed in the general population (Fig. 1A). Reaction product crystals from retrogradely transported horseradish peroxidase are visible in labeled TTMNs in the light microscope (Fig. 1B, inset) and in the electron microscope (Fig. 1B, C). Reaction product crystals extend from the soma into the proximal dendrites and there is also diffuse cytoplasmic darkening.

Synaptic Terminals that are Common on TTMNs

Terminals abut the TTMN somata and proximal dendrites; we studied those that formed synapses (shaded in colors on Figs. 1B, C, 2). There are few such terminals on the soma, covering only a small proportion of the total membrane (avg. 12.4%, range 5-29%, Table 1). Terminals on the proximal dendrites cover more of the membrane there (avg. 28.3%, range 22-33%, Table 1). Visual inspection of the synapses formed by the terminals suggests division into three types. The first type of synapse contains large, round vesicles (Lg Rnd, Fig. 2A). These synapses exhibit a distinct asymmetric postsynaptic density in the motoneuron. The second type contains smaller, round vesicles (Sm Rnd, Fig. 2B) and are also asymmetric. These terminals always contain, in addition to the clear synaptic vesicles, one or more dense core vesicles (Fig. 2B, avg. diam. 78.4 nm for 11 synapses). Dense core vesicles are usually observed near the plasma membrane in varying positions with respect to the active zones; they are infrequent and appear only in about every third section. In the third type of synapse, the vesicles have shapes that range from round to flat and will be termed “pleomorphic” (Pleo, Fig. 2C); their synaptic specializations have minimal postsynaptic densities (symmetric synapses).

Measurements of synaptic vesicles confirmed these different appearances. Vesicles measured from a single synapse (Fig. 3A, B) have a range of sizes and circularities (Fig. 3C), almost certainly because some vesicles appear in tangential section and because those that are flattened can appear circular in some orientations. In order to compare different terminals, we collapsed this variability by computing mean data (large dot in the center of Fig. 3C). Plots of mean data from all terminals are shown in Fig. 4, in which each point represents an individual terminal. There are three clusters of points that reflect our impression of the three vesicle types (Fig. 2). Using the *kmeans* analysis (see Methods) and an assumption of three clusters establishes the boundaries for the groups (color coding on Fig. 4). Terminals containing Pleo vesicles have mean circularities less than 0.85. Terminals containing Sm Rnd vesicles have higher mean circularities and mean areas less than 1,450 nm^2. The remaining terminals contain Lg Rnd vesicles. The Sm Rnd and Lg Rnd terminals have a significantly different mean vesicle area (*t* test, $P < 0.0001$). This separation is enhanced by an additional metric, whether or not the terminal contains a dense core vesicle (see key Fig. 4). All Sm Rnd terminals have dense core vesicles whereas most Lg Rnd terminals do not. In summary, the morphometric data confirm our impression that there are three common types of synapses on TTMNs.

Using serial sections, we often found that terminals gave rise to multiple synapses, and those from the same terminal were of the same type. In our morphometric data set, 31 of the terminals formed multiple synapses. Figure 4 used combined data from all synapses of a given terminal, but when plotted separately (data not shown), the data points from individual synapses of a single terminal always fell into just one of the three clusters. In two terminals, though, the data from one of the synapses fell into a borderline area. One of these was a Lg Rnd terminal: two of its synapses clearly fell into the Lg Rnd cluster (mean areas 1,601 and 1,646 nm^2) and the third synapse (mean area 1,437 nm^2) fell just beyond the border. No dense core vesicles were observed. The second of these was a Sm Rnd terminal: one of its synapses was in the middle of the Sm Rnd cluster (mean area 1,101 nm^2) whereas its other synapse (mean area 1,477 nm^2) was just beyond the border. Dense core vesicles were present in this terminal. Overall, though, the data suggest a terminal forms just a single type of synapse.

Only terminals with Pleo vesicles engulf and form synapses on spines from TTMN somata (Fig. 2C), or, in a single case, a TTMN dendrite. Eight of a total of 26 terminals with Pleo vesicles have spine-associated synapses and at least one such synapse was found on each of our six TTMNs. The spines are simple, unbranched tubes with diameters 0.4 μm or less and lengths 0.75 μm or less. Spines contained flocculent material but no mitochondria; three spines had a spine apparatus (Peters et al., 1991) in their proximal portion. We may have undercounted synapses with Pleo vesicles because the limited membrane associated with an engulfed spine made it hard to judge whether a cleft was formed and because there is minimal postsynaptic density.

A few terminals with Lg Rnd vesicles were distinct from most others of the group. These terminals were distinct because they were much bigger (Figs. 2, 5A) than the majority. These big terminals, though, did not form synapses that were different from the remainder of our sample of terminals with Lg Rnd vesicles. A few other terminals with Lg Rnd vesicles have a high content of neurofilaments and sometimes these, like the one illustrated in Fig. 5B, are big in size.

Synaptic Terminals that are Less Common

Two uncommon groups of terminals were so distinctive that we separated them from the common types. One of these has round vesicles of several sizes (Fig. 5C), so we call this type heterogeneous and round (Het Rnd). Most of the vesicles are about as big as Lg Rnd

vesicles and a few are much larger, reminiscent of such synapses on stapedius motoneurons (Lee et al., 2008). The large vesicles are not coated vesicles although coated vesicles were sometimes seen in all types of terminals. Our sample contains two synapses with Het Rnd vesicles, both on proximal dendrites, one forming two synapses (Table 1). Second, there were two terminals that had subsurface/subsynaptic cisterns in the postsynaptic membrane (Fig. 5D) of the TTMN somata. These Cistern (Cist) terminals also appear on other motoneurons (Conradi et al., 1979). At the bilaminar cistern, the pre- and postsynaptic membranes expand to form a cleft that has a small discontinuity (narrowing) near its center. These terminals also contain clear vesicles that are small (mean area 1,162 nm^2) and round, and each of them contains a dense core vesicle. The cistern illustrated (Fig. 5D) extended over 15 serial sections and its length in one of the sections was 0.71 μm. It had an en face area of 0.59 μm^2, which is by far the biggest specialization area of our sample.

Rarely found in the vicinity of TTMNs are axons that contain many dense core vesicles that are usually larger (≈ 115 nm diam., Fig. 5E) than the those described earlier. No synapses with TTMN membranes are observed with these axons; however, in one instance one of them contacted a TTMN.

Sometimes, the terminals that form synapses onto TTMNs also form synapses with unidentified dendrites in the neuropil (not shown), however no terminals were seen to receive synapses. None of the synapses were apposed by “Taxi” (postsynaptic dense) bodies (Conradi et al., 1979; Yang et al., 1997; Ichiyama et al., 2006) in the TTMN. Neuropil surrounding TTMNs (Figs. 1B, 2) includes many myelinated axons, some as large as 6 μm in diameter, as well as small, unmyelinated axons, dendrites, and axon terminals. The observed synapses, and the TTMNs themselves, are located in axodendritic neuropil among the axons.

Numbers of Synapses per Terminal and Sizes of Synpases

The numbers of synapses formed per terminal depended on terminal type, with the most synapses formed by terminals with Lg Rnd vesicles. An example of one of these terminals, which formed four synapses in the 20 sections examined, is shown in Fig. 6A). This terminal may have formed others because it extended beyond our sections (indicated by the figure’s dashed line at the terminal’s right edge). Another terminal, forming two synapses and containing Sm Rnd vesicles (Fig. 6B), also continued beyond our series. A third terminal containing Pleo vesicles (Fig. 6C) formed only one synapse, known because its apposition with the TTMN was completely sectioned (13 sections). In our material, a total of 36 terminals were sampled in more than 10 serial sections (Table 2). Although this is enough to only partially section through most of the terminals (see Table legend for exceptions), we used the available data to investigate whether there was a difference in the numbers of synapses formed. Terminals containing Lg Rnd vesicles form the highest number of synapses (avg. 2.73 synapses per terminal), with fewer formed by those containing Sm Rnd vesicles (avg. 1.58 synapses/terminal) or Pleo vesicles (avg. 1.22 synapses/terminal). In terms of the number of synapses formed per terminal, the three common terminal types are significantly different (Table 2 legend). Finally, two terminals containing Het Rnd vesicles, each observed in 12 sections, formed either 1 or 2 synapses.

In our sample, terminals with Lg Rnd vesicles were also on average bigger than the other types. Since entire terminals were not usually captured completely in our series, the sizes of terminals was quantified by measuring the lengths of their apposition with the TTMN in a section that contained the synapse (Fig. 6, dark lines show the sections used for apposition measurements). The measurements (Fig. 7A) indicate that terminals with Lg Rnd vesicles can have the longest apposition (up to 8.2 μm, Fig. 7A). These appositions averaged 2.26 μm (SE 0.36 μm), whereas those from Sm Rnd terminals averaged 1.14 μm (SE 0.07 μm)

and those from Pleo terminals averaged 1.24 μm (SE 0.18 μm). There was a significant difference between these appositions (analysis of variance (ANOVA) F=5.34, $P < 0.007$). Since some of these terminals were long and narrow (e.g., Fig. 1C, lower terminal), some of the lower data values may actually represent long terminals sectioned transverse to their long axes. We investigated whether the appositions were different for terminals on the soma vs. dendrites but there was no significant difference in our sample (Student t-Test, Lg Rnd P = 0.26, Sm Rnd P = 0.68, Pleo P = 0.29).

The area of the synapse also depends on the synapse type (Figs. 6, 7B). The areas of synapses having Lg Rnd vesicles are always less than 0.06 μm^2, whereas synapses with Sm Rnd and Pleo vesicles are usually larger. Synapses with Lg Rnd vesicles are present in at most four sections, but those having Sm Rnd and Pleo vesicles are so large that they often continue beyond the available sections, so data from many of these synapses could not be plotted. Synapses are almost always oval-shaped without perforations.

Relative Frequency of Terminal Types

The numbers of the synaptic terminals observed on each TTMN are listed in Table 1 and the overall percentages are plotted in Fig. 8A. For the sample of 79 synaptic terminals, the most common type have Lg Rnd vesicles (27 terminals, or 34.2% of the total). Of the remaining terminals, 22 (27.8%) have Sm Rnd vesicles and 26 (32.9%) have Pleo vesicles. All six TTMNs received at least one synapse from each of the three common types. We tested for differences in proportions of the three common types of synapse by comparing the percentages of terminals on the six individual neurons. The overall percentages were not significantly different from each other (Kruskal-Wallis, P = 0.73). Of the synaptic terminals, 38 are on somata and 41 are on proximal dendrites. For the common types of synapses, there was no significant difference in the percentages of terminal types on the somata versus on the dendrites (Kruskal-Wallis, P = 0.92).

We investigated whether the relative frequency of terminal types depended on the morphology of the TTMN. Labeled TTMNs were classified in the light microscope according to the criteria of Mukerji et al. (2009): “stellate” cells had three or more dendrites that projected from the cell body in different directions; “octopus-like” cells had dendrites projecting from one side of the cell body, and “fusiform” cells had narrow somata and dendrites projecting from opposing poles of the cell body. For example, the neurons illustrated in Fig. 1A were classified as fusiform (N3), octopus-like (N5), and stellate (N2, N1). The neuron illustrated in Fig. 1B, which had four dendrites, was classified as a “stellate” TTMN, and the neuron illustrated in Fig. 1C was classified as fusiform. Our sample of six neurons for which we have ultrastructural data (Table 1) consisted of two each of stellate (N1, N2), fusiform (N3, N4), and octopus-like (N5, N6). We considered the percentages of the common types of synapses onto these groups. There was no significant difference in percentage when the groups were compared (Kruskal-Wallis, P = 0.88) or when individual comparisons were made between the six neurons (Kruskal-Wallis, P = 0.82). Although our data are limited because of the small sample size, they suggest no difference in inputs to TTMNs of different shape.

DISCUSSION

Most Synapses on TTMNs have Excitatory Morphology

In this first report of the ultrastructure of synapses on TTMNs, we demonstrate the types of synaptic terminals that provide inputs to these neurons. The common types form asymmetric synapses associated with vesicles that are round (Lg Rnd, Sm Rnd, together 62% of the total synapses) or form symmetric synapses associated with vesicles that are pleomorphic (Pleo,

32.9% of the total). Additional types are present but uncommon, and distal dendrites have yet to be examined. The TTMN synaptic profile (Fig. 8A) is very similar to that found on stapedius motoneurons (Lee et al., 2008), except that stapedius motoneurons have even fewer terminals with Pleo vesicles (17.3%). Data from other motoneurons, including neurons in the nearby trigeminal motor nucleus, suggest a close correspondence between synapse type and transmitter types. Terminals that have asymmetric synapses associated with round vesicles are generally immunopositive for the excitatory neurotransmitter glutamate, whereas those that form symmetric synapses associated with pleomorphic or flat vesicles are generally immunopositive for the inhibitory transmitters gamma-amino butyric acid (GABA) or glycine or both (Bae et al., 1999; 2002; Paik et al., 2009). Our data thus suggest that a large majority of the synapses received by TTMNs are glutamatergic and excitatory.

These synapse types share general similarities with those on spinal α-motoneurons (Fig. 8B), but the proportions are different. In particular Pleo vesicle synapses, which probably correspond to those containing flattened vesicles (F) on spinal motoneuron, account for as much as 70% of all synapses on spinal motoneurons (Conradi et al., 1979; Kellerth et al., 1979; Ichiyama et al., 2006) and as much as 50% of the synapses on trigeminal motoneurons (Bae al., 2002). Neither the tensor tympani nor the stapedius muscles have antagonistic muscles, which perhaps explains the smaller numbers of synapses likely to be inhibitory on their motoneurons: the usual inhibitory pathway from an antagonistic muscle's neural system is apparently not present. For some motoneurons, input terminals from muscle spindle afferents receive presynaptic input (Bodian, 1975; Luo and Dessem, 1999). Middle ear muscles lack muscle spindles (van den Berge and van der Wal, 1990), and we did not find terminals that were presynaptic to other terminals. Clearly, the differences between middle ear and other motoneuron systems suggest differences in the way that middle ear muscles are controlled by the brain.

Separation of Synaptic Terminal Types

Our results using quantitative morphometry of synaptic vesicles indicate that terminal types can generally be distinguished by using average measures for area and circularity. This use reduces the wide ranges seen in vesicles from individual synapses, as observed here and previously (Satzler et al., 2002). Most previous studies used qualitative methods to distinguish terminal types (Lenn and Reese, 1966; Schwartz and Gulley, 1978; Cant and Morest, 1979; Conradi et al., 1979; Treeck and Pirsig, 1979; Schwartz, 1980; Cant, 1993; Benson et al., 1996; Rubio, 2004; Ichiyama et al., 2006; Lee et al., 2008). Our quantitative separation is an improvement over qualitative assessment, which may be affected by factors such as number of vesicles or packing density. The circularity measure has been used previously (Berrebi and Spirou, 1998), and has largely supplanted earlier approaches of "binning" individual vesicles by their individual shape. Such binning requires premeasurement establishment of cutoff values separating round from flat vesicles (Valdivia, 1971).

The k-means algorithm, with an assumption of three clusters, provided a separation of our data. We assumed three clusters because of our visual impression of three types of synapses and because our previous studies of stapedius motoneurons had found three common types. A further separation of round vs. Pleo vesicles is the degree of asymmetry of the synapse, but this characteristic was not necessary to achieve the separation boundary. A further separation between terminals containing Sm Rnd vs. Lg Rnd vesicles is the presence of a dense core vesicle, and this characteristic was important in providing separation here. Similar findings hold for stapedius motoneuron terminals (Lee et al., 2008). Serial sections are necessary to observe dense core vesicles since these vesicles are not contained in every section and could be missed by "survey" methods. Similarly, serial sections were important

in order to combine morphometric data from several synapses, because a few individual synapses gave borderline values for mean vesicle area. The vesicles of the Lg Rnd and Sm Rnd groups are statistically different in mean area, and the synaptic areas (Fig. 7B) and number of synapses per terminal (Table 2) are also different. Whether these differences result in a different form of excitatory neurotransmission is not clear. Different sizes of round vesicles have also been reported at other synapses (e.g., Treeck and Pirsig, 1979; Rubio et al., 2004; Matsuda et al., 2004). Finally, it would not be surprising if future studies were to form further subdivisions of terminals containing Lg Rnd vesicles, since these terminals are diverse in terms of their sizes, appositions, numbers of vesicles, and range of neurofilament content.

Inputs to TTMNs

The two types of round-vesicle inputs to TTMNs likely represent two different excitatory pathways, one mediating a reflexive contraction in response to sound and another mediating contraction accompanying voluntary movements (Salomon and Starr, 1963; Borg et al., 1984; Stach et al., 1984; Howell et al., 1986). For their sound-evoked reflex, TTMNs are reported to receive direct input from the cochlear nucleus (Itoh et al., 1986; Rouiller et al., 1986; Ito and Honjo, 1988; Billig et al., 2007). In order to determine which of the terminals of the present study correspond to these inputs, it would be necessary to label them with one tracer and label the TTMNs with a second tracer as was done previously by Itoh et al., 1986. Then, the TTMNs from these double-injections experiments could be examined in the electron microscope to determine which type of terminal was labeled. TTMNs also receive bilateral input from the superior olivary complex (Rouiller et al., 1986; Billig et al., 2007; Windsor et al., 2007), which, if excitatory, would contain round synaptic vesicles. In contrast, the neural circuitry associated with movement-associated contractions of the tensor tympani has not been worked out. TTMNs do receive inputs from the dorsolateral part of the oral pontine reticular formation (Li et al., 1995; Reuss et al., 2009). Such inputs, presumably excitatory, may cause the muscle to contract during vocalizations (Jürgens, 2009) and other movements.

Motoneurons supplying the tensor tympani as well as the stapedius receive fibers and endings that immunostain for a variety of neuromodulators including substance P (Reuss et al., 2008, 2009). Within synaptic terminals, substance P immunostaining is localized to dense core vesicles (Pickel et al., 1979; Merighi et al., 1991). The number of dense core vesicles within a terminal has been used to distinguish terminal types in the spinal cord, and a common type (S or simple terminals) contains small clear vesicles and only a few dense core vesicles (de Lanerolle and Lamotte, 1983; Lamotte and Shapiro, 1991). This type has similar morphology to the type we call Sm Rnd, and we suggest it corresponds to the substance-P positive terminals. Dense core vesicles may also deliver synapse-associated proteins such as piccolo and bassoon to the active zones (Ahmari et al., 2000; Zhair et al., 2001; Sorra et al., 2006).

Motoneurons supplying the middle ear muscles also receive endings that immunolabel for serotonin (Thompson et al., 1998). Ultrastructurally, serotonin-immunoreactive terminals contain clear vesicles and substantial numbers of dense core vesicles (Mollgard and Wiklund, 1979). They may correspond to the axons that we observed that contain many large dense core vesicles (Holtman et al., 1990). In other neural systems, some serotoninergic axon terminals form classical synapses (Maxwell et al., 2003), whereas others apparently do not (Schaffar et al., 1984), rather releasing serotonin into the extracellular space. The latter situation seems to apply to TTMNs, since they do not appear to receive classical synapses from axons containing many large dense core vesicles. The number of such endings close to each TTMN appears to be infrequent (Thompson et al., 1998), which corresponds to our finding that these axons are uncommon. The function of this innervation

is speculative, but it may modulate the middle ear muscle reflex to sound according to the sleep/wake cycle (Stegel et al., 1991). TTMNs also receive some endings that stain for tyrosine hydroxylase (Reuss et al., 2009). At the ultrastructural level, they are expected to contain numerous dense core vesicles (Groves and Wilson, 1980; Peters et al., 1991) and may also correspond to the axons that we observed that contain many large dense core vesicles. Overall, the diversity of terminals on TTMNs allows for these motoneurons to be controlled by a variety of inputs in addition to the major sound-evoked and volitional excitatory pathways.

Acknowledgments

The authors thank Drs. John J. Guinan, Jr. and M. Charles Liberman for reviewing previous versions of this manuscript, Dr. Wen Xu for technical assistance with this work, and Amelie Guex for help with the MATLAB *kmeans* implementation. Preliminary results of this study were presented in abstract form at the Association for Research in Otolaryngology Midwinter Meetings, February, 2008 and February, 2009.

Grant sponsor: National Institutes of Health-NIDCD; Grant number: DC06285 (to D.J.L.) and DC01089 (to M.C.B.).

LITERATURE CITED

Ahmari S, Buchanan J, Smith S. Assembly of presynaptic active zones from cytoplasmic transport packets. Nat Neurosci. 2000; 3:445–451. [PubMed: 10769383]

Bae YC, Tatsuzo N, Ihn HJ, Choi MH, Yoshida A, Moritani M, Shiho H, Shigenaga Y. Distribution pattern of inhibitory and excitatory synapses in the dendritic tree of single masseter alpha-motoneurons in the cat. J Comp Neurol. 1999; 414:454–468. [PubMed: 10531539]

Benson TE, Berglund AM, Brown MC. Synaptic input to cochlear-nucleus dendrites that receive medial olivocochlear synapses. J Comp Neurol. 1996; 365:27–41. [PubMed: 8821439]

Berrebi AS, Spirou GA. PEP-19 immunoreactivity in the cochlear nucleus and superior olive of the cat. Neuroscience. 1998; 83:535–554. [PubMed: 9460761]

Billig I, Yeager MS, Blikas A, Raz Y. Neurons in the cochlear nuclei controlling the tensor tympani in the rat: a study using pseudorabies virus. Brain Res. 2007; 1154:124–136. [PubMed: 17482147]

Bodian D. Origin of specific synaptic types in the motoneuron neuropil of the monkey. J Comp Neurol. 1975; 159:225–244. [PubMed: 1112912]

Borg, E.; Counter, SA.; Rosier, G. Theories of middle ear muscle functions. In: Silman, S., editor. The acoustic reflex: basic principles and clinical applications. Academic Press; Orlando: 1984. p. 63-101.

Cant, NB. The synaptic organization of the ventral cochlear nucleus of the cat: the peripheral cap of small cells. In: Merchan, MA.; Juiz, JM.; Godfrey, DA.; Mugnaini, E., editors. The mammalian cochlear nuclei: organization and function. Plenum Press; New York: 1993. p. 91-106.

Cant NB, Morest DK. Organization of the neurons in the anterior division of the anteroventral cochlear nucleus of the cat. Light microscopic observations. Neuroscience. 1979; 4:1909–1923. [PubMed: 530438]

Conradi S, Kellerth JO, Berthold CH. Electron microscopic studies of serially sectioned cat spinal alpha-motoneurons. II. A method for the description of architecture and synaptology of the cell body and proximal dendritic segments. J Comp Neurol. 1979; 184:741–754. [PubMed: 422760]

de Lanerolle NC, Lamotte CC. Ultrastructure of chemically defined neuron systems in the dorsal horn of the monkey. I. Substance P immunoreactivity. Brain Res. 1983; 274:31–49. [PubMed: 6193842]

Doucet JR, Lenhan NM, May BJ. Commissural neurons in the rat ventral cochlear nucleus. J Assoc Res Otolaryngol. 2009; 10:269–280. [PubMed: 19172356]

Fifková E, Eason H, Schaner P. Inhibitory contacts on dendritic spines of the dentate fascia. Brain Res. 1992; 577:331–336. [PubMed: 1606504]

Gelfand, S. The contralateral acoustic reflex. In: Silman, S., editor. The acoustic reflex: basic principles and clinical applications. Academic Press; Orlando: 1984. p. 137-186.

Groves PM, Wilson CJ. Monoaminergic presynaptic axons and dendrites in rat locus coeruleus seen in reconstructions of serial sections. J Comp Neurol. 1980; 193:853–852. [PubMed: 7430441]

Henry MA, Westrum LE, Johnson LR. Enhanced ultrastructural visualization of the horseradish peroxidase-tetramethylbenzidine reaction product. J Histochem Cytochem. 1985; 33:1256–1259. [PubMed: 4067278]

Holtman JR Jr, Vascik DS, Maley BE. Ultrastructural evidence for serotonin-immunoreactive terminals contacting phrenic motoneurons in the cat. Exp Neurol. 1990; 109:269–272. [PubMed: 2209771]

Horner KC. The tensor tympani reflex in the mouse. Hearing Res. 1986; 24:117–123.

Howell P, Marchbanks RJ, El-Yaniv N. Middle ear muscle activity during vocalization in normal speakers and stutterers. Acta Otolaryngol. 1986; 102:396–402. [PubMed: 3788538]

Ichiyama RM, Broman J, Edgerton VR, Havton LA. Ultrastructural synaptic features differ between the alpha- and gamma-motoneurons innervating the tibialis anterior muscle in the rat. J Comp Neurol. 2006; 499:306–315. [PubMed: 16977622]

Ito J, Honjo I. Electrophysiological and HRP studies of the direct afferent inputs from the cochlear nuclei to the tensor tympani muscle motoneurons in the cat. Acta Otolaryngol. 1988; 105:292–296. [PubMed: 3389115]

Itoh K, Nomura S, Konishi A, Yasui Y, Sugimoto T, Muzino N. A morphological evidence of direct connections from the cochlear nuclei to TTMNs in the cat: a possible afferent limb of the acoustic middle ear reflex pathways. Brain Res. 1986; 375:214–219. [PubMed: 2424568]

Jones EG, Powell TPS. Morphological variations in the dendritic spines of the neocortex. J Cell Sci. 1969; 5:509–529. [PubMed: 5362339]

Jürgens U. The neural control of vocalization in mammals: a review. J Voice. 2009; 23:1–10. [PubMed: 18207362]

Kellerth JO, Berthold CH, Conradi S. Electron microscopic studies of serially sectioned cat spinal alpha-motoneurons. III. Motoneurons innervating fast-twitch (type FR) units of the gastrocnemius muscle. J Comp Neurol. 1979; 184:755–767. [PubMed: 84821]

Lamotte CC, Shapiro CM. Ultrastructural localization of substance P, Met-enkephalin, and somatostatin immunoreactivity in lamina X of the primate spinal cord. J Comp Neurol. 1991; 306:290–306. [PubMed: 1711056]

Lee DJ, Benson TE, Brown MC. Diverse synaptic terminals on rat stapedius motoneurons. J Assoc Res Otolaryngol. 2008; 9:321–333. [PubMed: 18563488]

Lenn NJ, Reese TS. The fine structure of nerve endings in the nucleus of the trapezoid body and the ventral cochlear nucleus. Am J Anat. 1966; 118:375–390. [PubMed: 5917192]

Li Y-Q, Takada M, Kaneko T, Noboru M. Premotor neurons for trigeminal motor nucleus neurons innervating the jaw-closing and jaw-opening muscles: differential distribution in the lower brainstem of the rat. J Comp Neurol. 1995; 356:563–579. [PubMed: 7560267]

Luo P, Dessem E. Ultrastructural anatomy of physiologically identified jaw-muscle spindle afferent terminations onto retrogradely labeled jaw-elevator motoneurons in the rat. J Comp Neurol. 1999; 406:384–401. [PubMed: 10102503]

Matsuda S, Kobayashi Y, Ishizuka N. A quantitative analysis of the laminar distribution of synaptic boutons in field CA3 of the rat hippocampus. Neurosci Res. 2004; 49:241–252. [PubMed: 15140566]

Maxwell DJ, Kebb R, Rashid S, Anderson E. Characterisation of axon terminals in the rat dorsal horn that are immunopositive for serotonin 5-HT_3A receptor subunits. Exp Brain Res. 2003; 149:114–124. [PubMed: 12592509]

Merighi A, Polak JM, Theodosis DT. Ultrastructural visualization of glutamate and aspartate immunoreactivities in the rat dorsal horn, with special reference to the co-localization of glutamate, substance P and calcitonin-gene related peptide. Neurosci. 1991; 40:67–80.

Mollgard K, Wiklund L. Serotoninergic synapses on ependymal and hypendymal cells of the rat subcommissural organ. J Neurocytol. 1979; 8:445–467. [PubMed: 490190]

Møller, A. Neurophysiological basis of the acoustic middle-ear reflex. In: Silman, S., editor. The acoustic reflex: basic principles and clinical applications. Academic Press; Orlando: 1984. p. 1-35.

Montero RS, Bribiesca E. State of the art of compactness and circularity measures. Int Math Forum. 2009; 4:1305–1335.

Mukerji S, Brown MC, Lee DJ. A morphologic study of Fluorogold labeled tensor tympani motoneurons in mice. Brain Res. 2009; 1278:59–65. [PubMed: 19397898]

Olucha F, Martinez-Garcia F, Lopez-Garcia C. A new stabilizing agent for the tetramethyl benzidine (TMB) reaction product in the histochemical detection of horseradish peroxidase (HRP). J Neurosci Meth. 1985; 13:131–138.

Örnung G, Ottersen O, Cullheim S, Ulfhake B. Distribution of glutamate-, glycine- and GABA-immunoreactive nerve terminals on dendrites in the cat spinal motor nucleus. Exp Brain Res. 1998; 118:517–532. [PubMed: 9504847]

Paik SK, Lee HJ, Choi MK, Cho YS, Park MJ, Moritani M, Yoshida A, Kim YS, Bae YC. Ultrastructural analysis of glutamate-, GABA-, and glycine-immunopositive boutons from supratrigeminal premotoneurons in the rat trigeminal motor nucleus. J Neurosci Res. 2009; 87:1115–1122. [PubMed: 19006082]

Peters, A.; Palay, SL.; Webster, H deF. The fine structure of the nervous system. Oxford; New York: 1991.

Pickel VM, Joh TH, Reis DJ, Leeman SE, Miller RJ. Electron microscopic localization of substance P and enkephalin in axon terminals related to dendrites of catecholaminergic neurons. Brain Res. 1979; 160:387–400. [PubMed: 33743]

Reuss S, Al-Butmeh S, Riemann R. Motoneurons of the stapedius muscle in the guinea pig middle ear: afferent and efferent transmitters. Brain Res. 2008; 1221:59–65. [PubMed: 18554578]

Reuss S, Kuhn I, Windoffer I, Riemann R. Neurochemistry of identified motoneurons of the tensor tympani muscle in rat middle ear. Hear Res. 2009; 248:69–79. [PubMed: 19126425]

Relkin EM, Sterns W, Azeredo WJ, Prieve BA, Woods CI. Physiological mechanisms of onset adaptation and contralateral suppression of DPOAEs in the rat. J Assoc Res Otolaryngol. 2005; 6:119–135. [PubMed: 15952049]

Rouiller EM, Capt M, Dolivo M, de Ribaupierre F. Tensor tympani reflex pathways studied with retrograde horseradish peroxidase and transneuronal viral tracing techniques. Neurosci Lett. 1986; 72:247–252. [PubMed: 3029633]

Rubio ME. Differential distribution of synaptic endings containing glutamate, glycine, and GABA in the rat dorsal cochlear nucleus. J Comp Neurol. 2004; 477:253–272. [PubMed: 15305363]

Sakai T. Relation between thickness and interference colors of biological ultrathin section. J Electron Microsc. 1980; 29:369–375.

Salomon G, Starr A. Electromyography of middle ear muscles in man during motor activities. Acta Neurol Scand. 1963; 39:161–168. [PubMed: 13991171]

Satzler K, Sohl LF, Bollmann JH, Borst JG, Frotscher M, Sakman B, Lubke JHR. Three-dimensional reconstruction of a calyx of Held and its postsynaptic neuron in the medial nucleus of the trapezoid body. J Neurosci. 2002; 22:10567–10579. [PubMed: 12486149]

Schaffar N, Jean A, Calas A. Radioautographic study of serotoninergic axon terminals in the rat trigeminal motor nucleus. Neurosci Lett. 1984; 44:31–36. [PubMed: 6717849]

Schwartz AM, Gulley RL. Non-primary afferents to the principal cells of the rostral anteroventral cochlear nucleus of the guinea-pig. Am J Anat. 1978; 153:489–508. [PubMed: 727150]

Schwartz IR. The differential distribution of synaptic terminal on marginal and central cells in the cat medial superior olivary nucleus. Am J Anat. 1980; 159:25–31. [PubMed: 7446440]

Shaw MD, Baker R. The locations of stapedius and tensor tympani motoneurons in the cat. J Comp Neurol. 1983; 216:10–19. [PubMed: 6306062]

Smith PH, Joris PX, Carney LH, Yin CTC. Projections of physiologically characterized globular bushy cell axons from the cochlear nucleus of the cat. J Comp Neurol. 1991; 304:387–407. [PubMed: 2022755]

Sorra K, Mishra A, Kirov SA, Harris KM. Dense core vesicles resemble active-zone transport vesicles and are diminished following synaptogenesis in mature hippocampal slices. Neurosci. 2006; 141:2097–2106.

Spangler KM, Henkel CK, Miller IJ Jr. Localization of the motor neurons to the tensor tympani muscle. Neurosci Lett. 1982; 32:23–27. [PubMed: 6183622]

Spirou GA, Brownell WE, Zidanic M. Recordings from cat trapezoid body and HRP labeling of globular bushy cell axons. J Neurophysiol. 1990; 63:1169–1190. [PubMed: 2358868]

Stach BA, Jerger JF, Jenkins HA. The human acoustic tensor tympani reflex. A case report. Scand Audiol. 1984; 13:93–99. [PubMed: 6463558]

Stegel DE, Benson KL, Zarcone VP Jr. Schubert ED. Middle-ear muscle activity (MEMA) and its association with motor activity in the extremities and head in sleep. Sleep. 1991; 14:454–459. [PubMed: 1759098]

Strutz J, Münker G, Zöllner C. The motor innervation of the tympanic muscles in the guinea pig. Arch Otorhinolaryngol. 1988; 245:108–111. [PubMed: 3390073]

Thompson AM, Thompson GC, Britton BH. Serotoninergic innervation of stapedial and tensor tympani motoneurons. Brain Res. 1998; 787:175–178. [PubMed: 9518599]

Torrealba F, Carrasco M. A review on electron microscopy and neurotransmitter systems. Brain Res Rev. 2004; 47:5–17. [PubMed: 15572159]

Valdivia O. Methods of fixation and the morphology of synaptic vesicles. J Comp Neurol. 1971; 142:257–274. [PubMed: 4105287]

Treeck H-H, Pirsig W. Differentiation of nerve endings in the cochlear nucleus on morphological and experimental basis. Acta Otolaryngol. 1979; 87:47–60. [PubMed: 760377]

Uchizono K. Characteristics of excitatory and inhibitory synapses in the central nervous system of the cat. Nature. 1965; 207:642–643. [PubMed: 5883646]

van den Berge H, Kingma H, Kluge C, Marres E. Electrophysiological aspects of the middle ear muscle reflex in the rat: latency, rise time and effect on sound transmission. Hear Res. 1990; 48:209–219. [PubMed: 2272930]

van den Berge H, van der Wal JC. The innervation of the middle ear muscles of the rat. J Anat. 1990; 170:99–109. [PubMed: 2254173]

Wang S-F, Spencer RF. Morphology and soma-dendritic distribution of synaptic endings from the rostral interstitial nucleus of the medial longitudinal fasciculus (riMLF) on motoneurons in the oculomotor and trochlear nuclei in cat. J Comp Neurol. 1996; 366:149–162. [PubMed: 8866851]

Windsor A, Roska B, Brown MC, Lee DJ. Transneuronal analysis of the middle ear muscle reflex pathways using pseudorabies virus. Assoc Res Otolaryngol. 2007 Abstr 605.

Yang H-U, Appenteng K, Balten TFC. Ultrastructural subtypes of glutamate-immunoreactive terminals on rat trigeminal motoneurones and their relationships with GABA-immunoreactive terminals. Exp Brain Res. 1997; 114:99–116. [PubMed: 9125455]

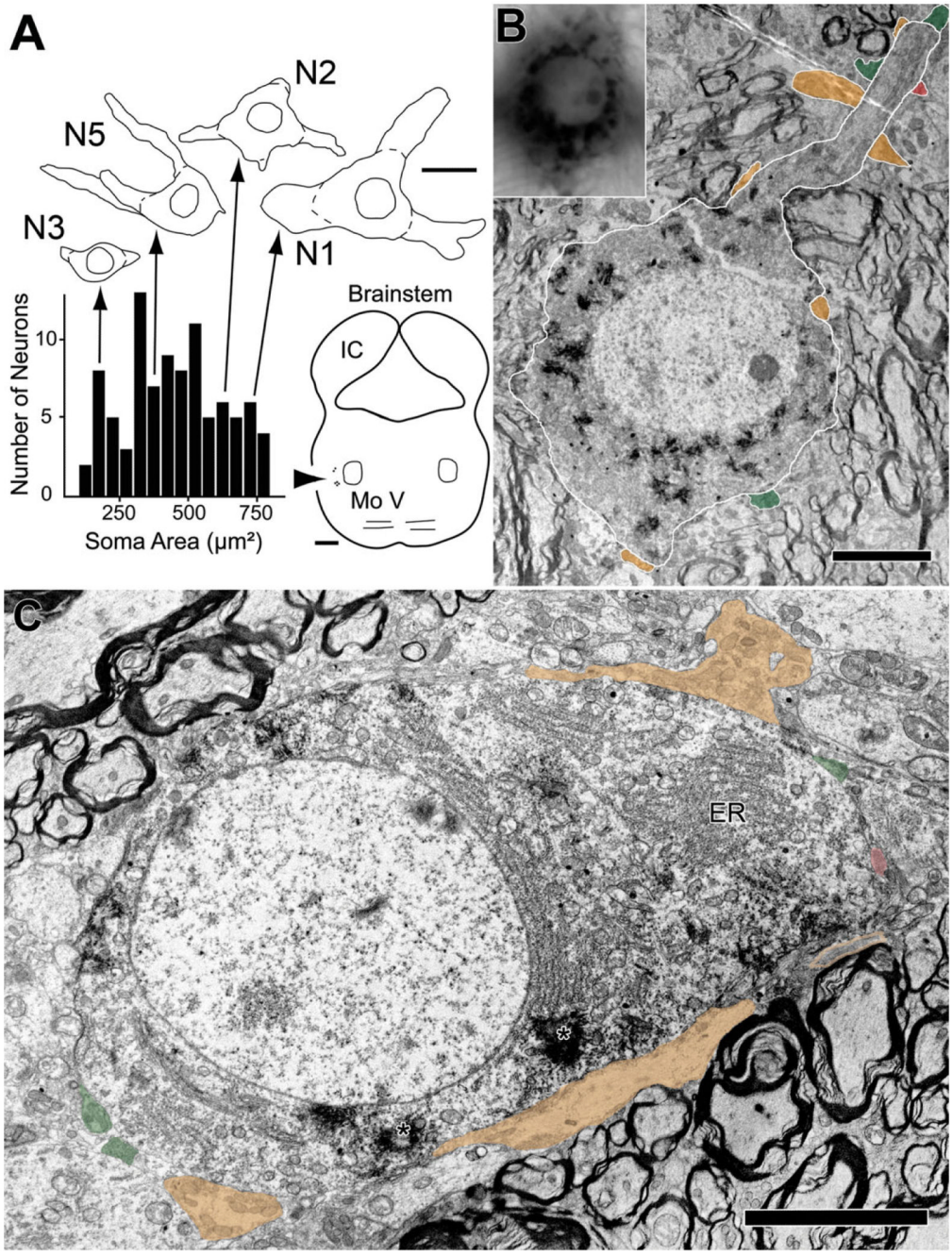

Fig. 1.

Example labeled TTMNs and their synaptic terminals. **A**: Plot of the soma areas of 92 labeled TTMNs. Above the plot are drawings of four of the TTMNs studied extensively in the electron microscope (Table 1). On the drawings, dashed lines indicate the outlines of the somata used for measurements. Arrows indicate where their soma areas fall on the plot; these areas span those seen in the general population. Scale bar: 25 μm. Brainstem outline at lower right shows the positions of the labeled neurons (arrowhead) relative to the trigeminal motor nucleus (Mo V). Scale bar: 1 mm. **B**: Low power electron micrograph of TTMN N2 (outlined in white) with numerous reaction product crystals in the cytoplasm. Inset at upper

left is a light micrograph of the same motoneuron. Similarities of the neuron in the two micrographs include distribution of black reaction product and the position of the nucleolus. Three other dendrites (faintly illustrated in the inset) are seen extending in different directions from this neuron. Synaptic terminals (colored) are seen on the soma (three terminals) and on the proximal dendrite (seven terminals). Scale bar = 5 μm. **C**: Low power electron micrograph of TTMN N4, showing reaction product crystals in the cytoplasm (asterisks). One proximal dendrite, just beginning to emerge from the soma, is identified as a dendrite because of the orientation of rough endoplasmic reticulum (ER) perpendicular to the nuclear membrane. Synaptic terminals are colored. One terminal (orange) between the TTMN and the scale bar is exceptionally large and consists in this section of two separate segments – the segment at the right has orange outlines because it does not contact the TTMN until deeper sections. Scale bar = 5 μm.

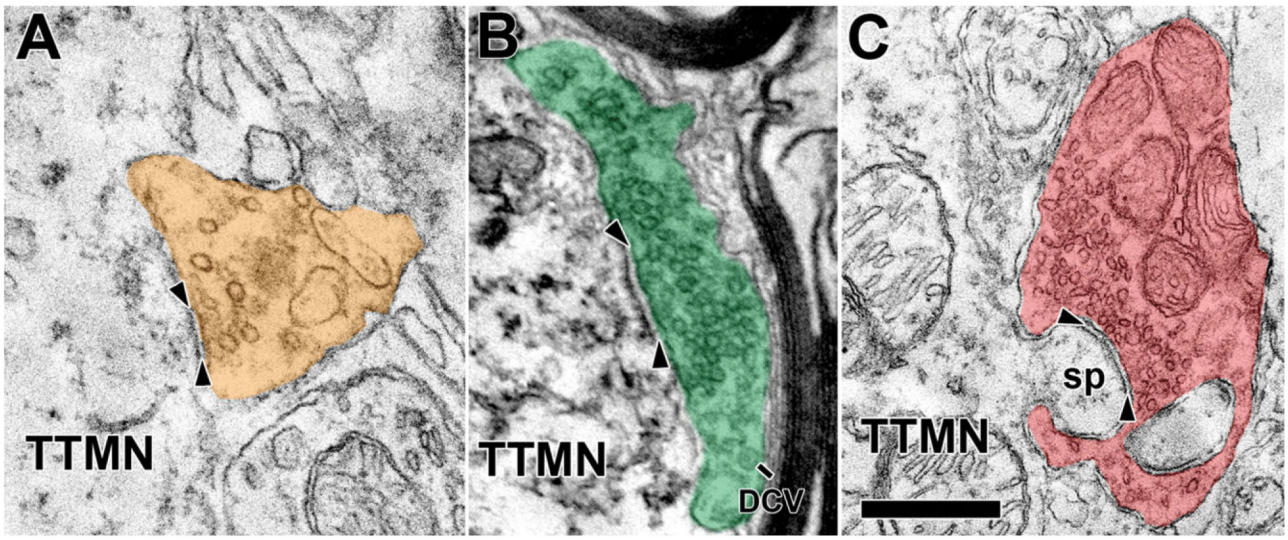

Fig. 2.

Examples synaptic terminals on TTMNs that illustrate the synaptic vesicles. The vesicles contained in the terminal in **A** are large and round (Lg Rnd), those in the terminal in **B** are smaller and round (Sm Rnd), and those in the terminal in **C** are pleomorphic (Pleo). As illustrated, our criteria for synapses requires a cleft between pre- and postsynaptic membrane (arrowheads), postsynaptic dense material, and synaptic vesicles. The terminal in B has a dense core vesicle (DCV). The terminal in C is associated with a TTMN spine (sp), curved in this case, and seen in two parts as it invaginates the terminal. Scale bar = 0.5 μm.

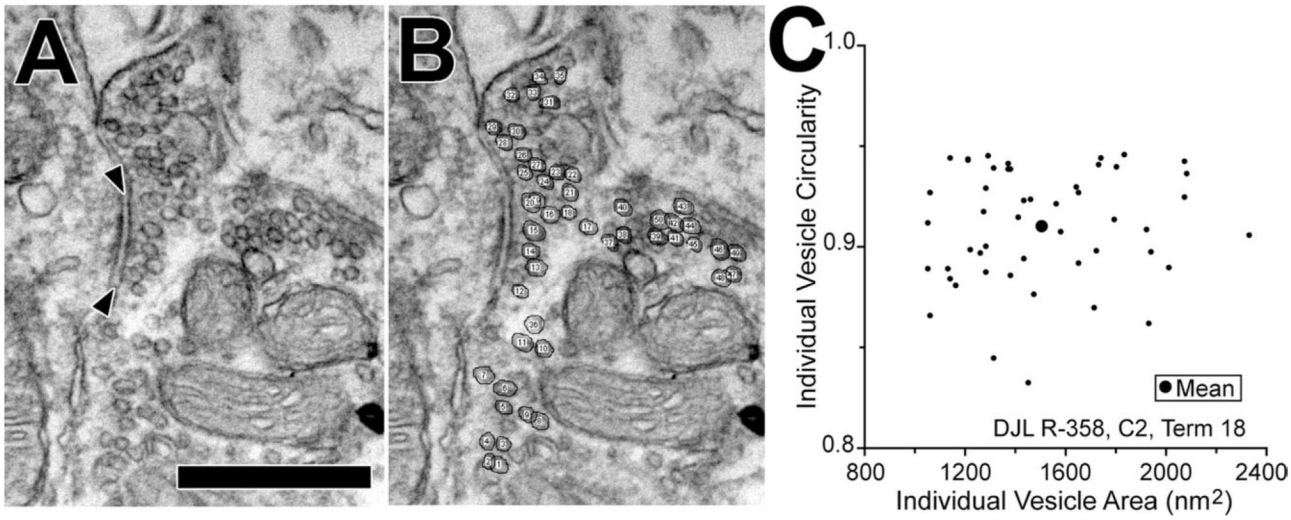

Fig. 3.

Vesicle measurements at a synapse on TTMN N2. **A**: Electron micrograph of the synapse (arrowheads) showing the clear synaptic vesicles packed within the terminal. Scale bar = 0.5 μm. **B**: Same micrograph after vesicles were circled and numbered. C: Scatter plot of the circularity vs. area for 47 individual clear vesicles in B. The large dot shows the mean area and mean circularity. Mean data like these were used to compare synapses (see Fig. 4).

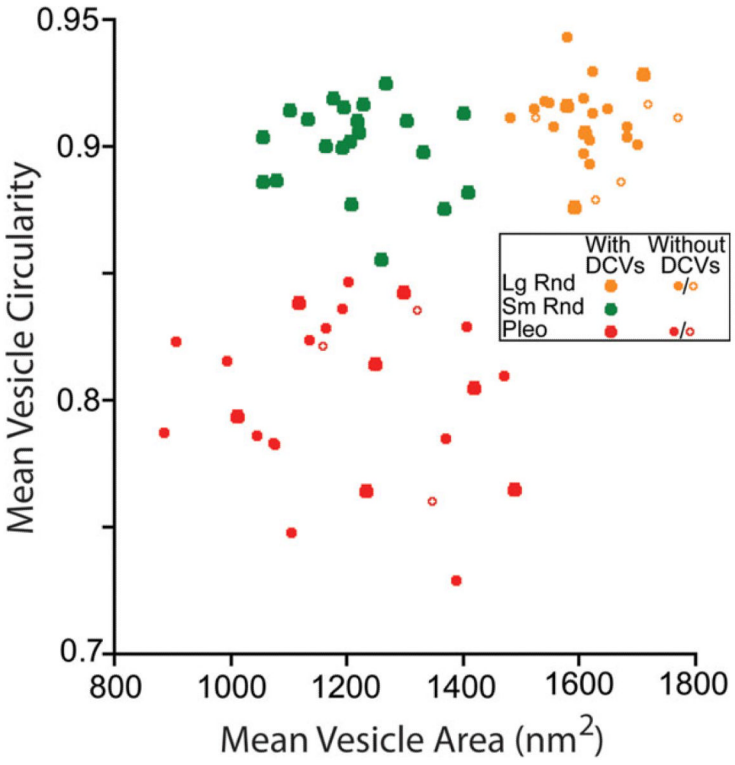

Fig. 4.

Plots of mean vesicle circularity versus mean vesicle area for the three common types of synapses on TTMNs. Each point represents measurements from all synapses of a single terminal. Symbol size distinguishes terminals with or without dense core vesicles (DCVs, see key), with open symbols representing terminals in which those vesicles were not seen but for which four or fewer sections are available. Color coding indicates cluster as identified by the kmeans algorithm. The centroids of the clusters were: Lg Rnd (1,615, 0.91), Sm Rnd (1,213, 0.90), and Pleo (1,199, 0.80). Het Rnd and Cist terminals (see Fig. 5) were not plotted.

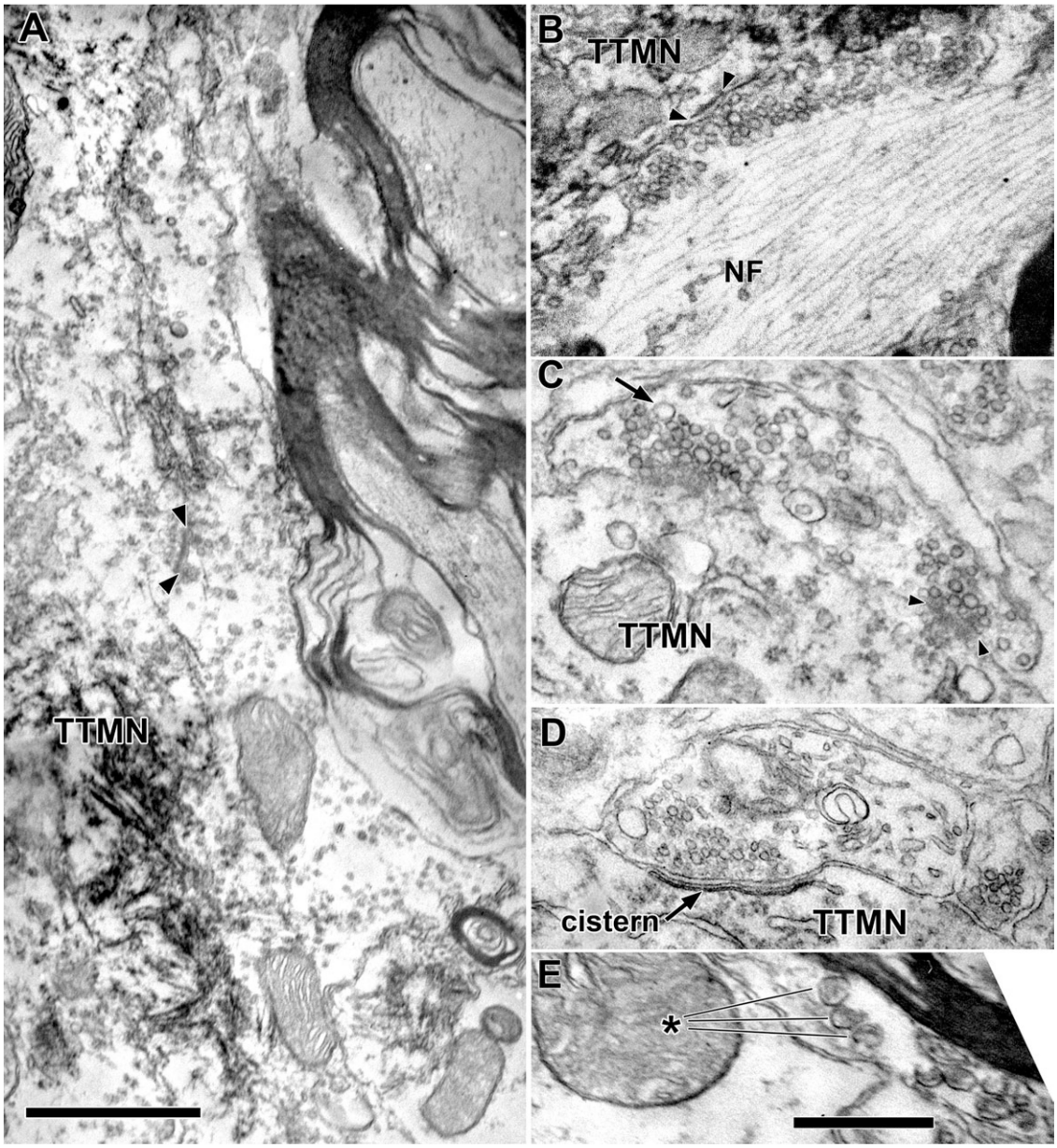

Fig. 5.

Examples of less common types of terminals on and near TTMNs. **A**: Electron micrograph of a terminal containing Lg Rnd vesicles that apposes the TTMN for over 6 μm, one of the longest appositions in our study. A synapse is denoted by the arrowheads. Scale bar = 1 μm. **B**: Terminal with Lg Rnd vesicles with a high neurofilament (NF) content. This terminal appears as the exceptionally large terminal of Fig. 3 and the NF content is high throughout the terminal. **C**: Terminal that has round vesicles of heterogeneous size (Het Rnd). Most vesicles are comparable to Lg Rnd vesicles but a few are quite large (arrow). A synapse is indicated with arrowheads. **D**: A Cist terminal with a bi-laminar cistern rather than a postsynaptic density in the adjacent portion of the motoneuron. The terminal contains round vesicles. **E**: Unmyelinated axon containing dense core vesicles (about eight in total, asterisk points to three) that are larger than those in other terminals. This axon was not observed to

contact a labeled TTMN (nearest TTMN was 1.9 μm away, out of the frame of this micrograph). Scale bar = 0.5 μm for B-E.

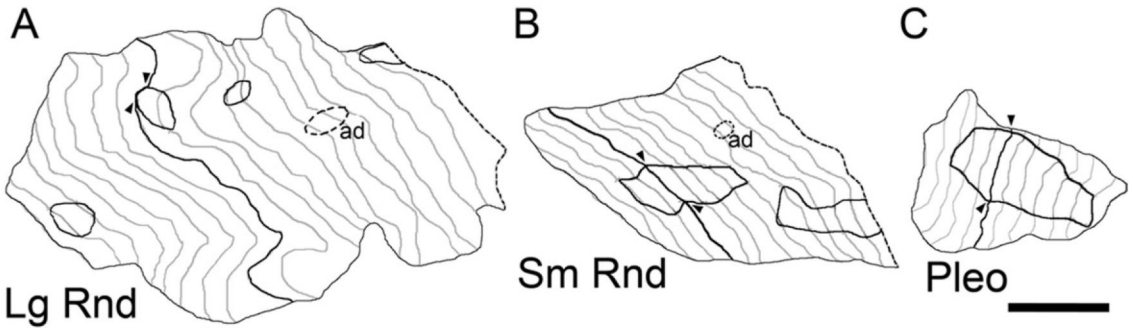

Fig. 6.

Three synaptic terminals in *en face* representations of their appositions with TTMNs. **A**: Lg Rnd; **B**: Sm Rnd; **C**: Pleo. The apposition is drawn for individual sections (in gray lines plus one dark line for the section used for apposition measurement) and each is staggered from the next by the section thickness (80 nm). Darkly outlined areas indicate locations of synapses (shown for single sections by arrowheads) and dashed areas indicate adherens junctions (ad). A smooth contour is used between adjacent sections. The number of sections available for the Lg Rnd terminal is 21, for the Sm Rnd terminal is 13, and for the Pleo terminal is 13. Dashed lines for the right-most sections of the Lg Rnd and Sm Rnd terminals indicate that the apposition appeared to extend beyond our series of sections. Scale bar: 0.5 um.

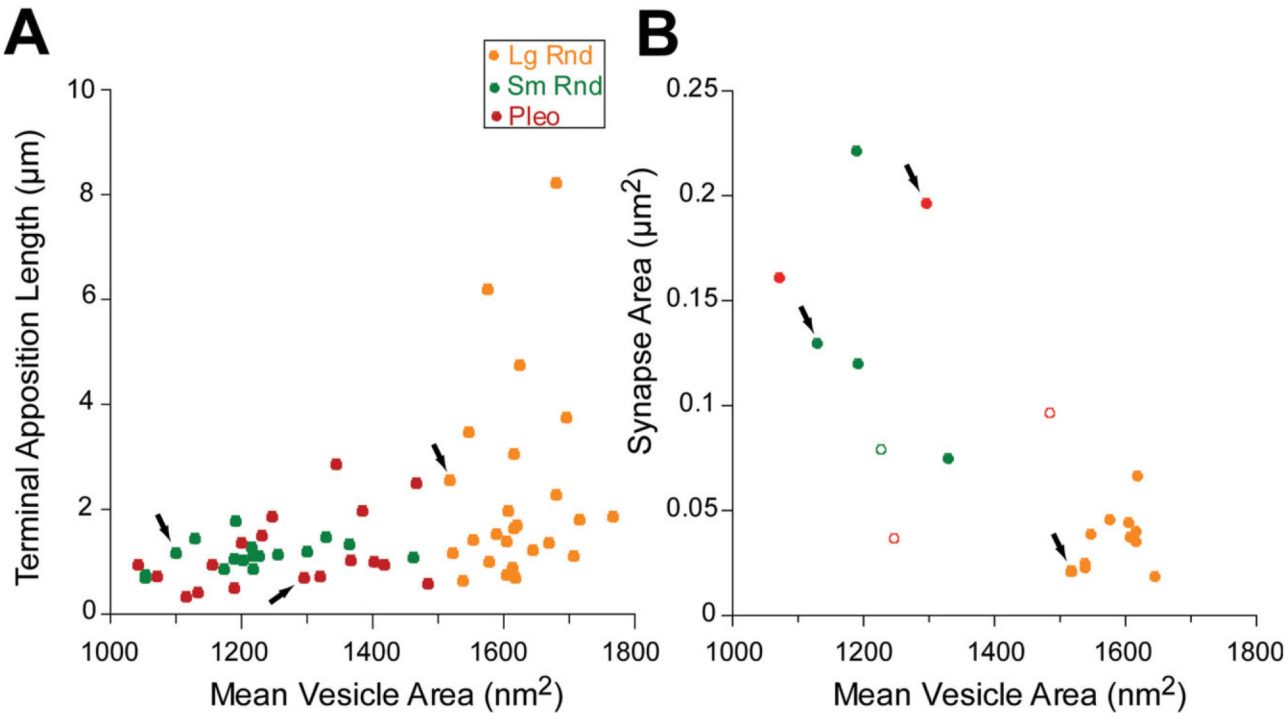

Fig. 7.

Plots of TTMN terminal apposition length (**A**) and synapse area (**B**). Arrows indicate the data points corresponding to the terminals in Fig. 6. Data in B are from all 19 synapses that are completely sectioned. Here, solid symbols represent synapses where the first and last parts were included in the series, whereas three open symbols denote where a section is missing at one end of the synapse (and thus represent a least estimate of their areas because the next section contains no synapse).

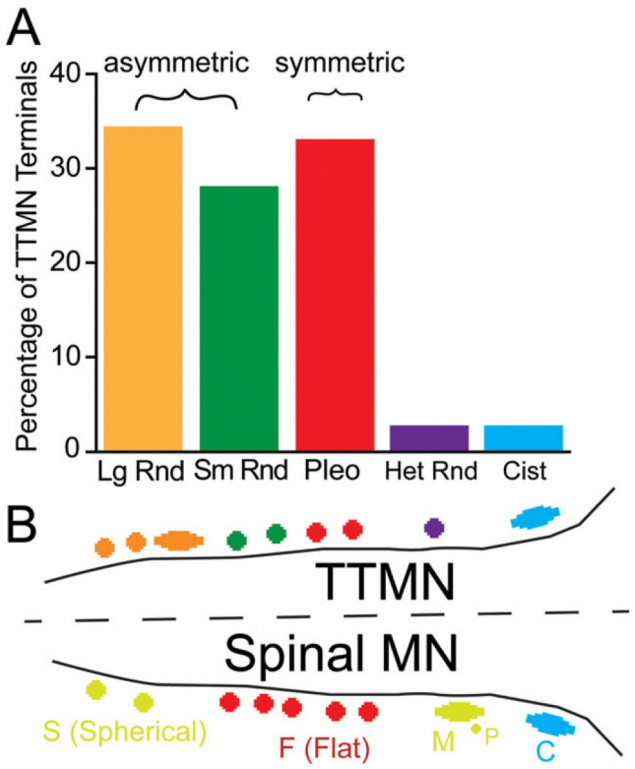

Fig. 8.

A: Percentages of each type of synaptic terminal on all six TTMNs examined in the electron microscope. Lg Rnd-Large Round; Sm Rnd-Small Round; Pleo-Pleomorphic; Het Rnd-Heterogeneous Round; Cist-Cistern. Brackets indicate the synaptic types that are asymmetric (having a prominent postsynaptic density) and those that are symmetric (having minimal postsynaptic density). **B**: Schematic of synaptic terminal types found on TTMNs, and comparison to types found on spinal α-motoneurons (after Conradi et al., 1979). Apparent correspondences are indicated with similar colors. S: spherical-vesicle synaptic terminals; M: large terminals containing spherical vesicles that receive input from other, presynaptic (P) terminals, or which have a synaptic complex with six or more “Taxi” bodies; F: flattened-vesicle synaptic terminals; C: cistern synaptic terminals.

TABLE 1
TTMNs and their Synaptic Terminals

	Soma/ Dend	# secs	% cov.	Terminals (Synapses)				
				Lg Rnd	Sm Rnd	Pleo	Het Rnd	Cist
Neuron								
N1	Soma	24	10	4 (4)	3 (3)	4 (6)		
	Dend		22	7 (13)	2 (3)	7 (8)	1 (2)	
N2	Soma	25	9	1 (3)	1 (1)	1 (1)		
	Dend		29	5 (11)	5 (7)	3 (3)	1 (1)	
N3	Soma	51	5	4 (8)	2 (4)	3 (3)		1 (1)
N4	Soma	16	29	2 (8)	3 (3)	2 (2)		1 (1)
	Dend		33	1 (5)	1 (3)	3 (3)		
N5	Dend	22	29	1 (4)	3 (5)	1 (2)		
N6	Soma	5	9	2 (3)	2 (3)	2 (2)		
Total			Avg.	Totals				
6	Soma		12.4% (SE 2.3%)	13 (26)	11 (14)	12 (14)		2 (2)
	Dend		28.3% (SE 2.3%)	14 (33)	11 (18)	14 (16)	2 (3)	
	Combined			27 (59)	22 (32)	26 (30)	2 (3)	2 (2)

Terminal counts are different from synapse counts (in parentheses) because multiple synapses can arise from the same terminal (e.g., Lg Rnd in Fig. 7). Data are separated for synapses on the soma vs. the proximal dendrite (Dend).

TABLE 2
Number of Terminals Containing Multiple Synapses

		Lg Rnd	Sm Rnd	Pleo	Het Rnd	Cist
Containing	1 synapse:	3	5	7	1	1
	2 synapses:	5	7	2	1	
	3 synapses:	3				
	4 synapses:	1				
	5 synapses:	3				
	Total:	15	12	9	2	1
	Avg. synapses/ terminal:	2.73	1.58	1.22	1.5	1
	SE:	0.39	0.16	0.16		

Data are from terminals in which 10 or more serial sections were examined. The average synapses/terminal was significantly different in a comparison of Lg Rnd, Sm Rnd, and Pleo types (Kruskal-Wallis, P=0.004). Although most terminals extended beyond our sections, two terminals containing Lg Rnd vesicles were completely sectioned and one formed five synapses and the other formed one synapse. One terminal containing Sm Rnd vesicles was completely sectioned and it formed two synapses. Three terminals containing Pleo vesicles were completely sectioned and each formed one synapse.